Earthquake Engineering and Engineering Seismology
Volume 2, Number 2, September 2000, pp. 1-14

Source Model for Simulating Ground Motion During the 1999 Chi-Chi Earthquake

K. Irikura [1] K. Kamae [2] L.A. Dalguer[1]

1) *Disaster Prevention Research Institute, Kyoto University, Uji, Kyoto 611-0011, irikura@egmdpri01.dpri.kyota-u.ac.jp, kamae@kuca.rri.kyoto-u.ac.jp*

2) *Reactor Research Institute, Kyoto University, Kumatori, Sennan, Osaka 590-0451, dalguer@egmdpri01.dpri.kyota-u.ac.jp*

ABSTRACT

Strong ground motions obtained during the 1999 Chi-Chi earthquake are characterized by larger motions in the hanging wall side than in the footwall side and also larger velocities and displacements at the northern part than at the southern part of the causative fault. We successfully simulated dynamic rupture process on the fault plane and strong ground motion in near-source area using the 2D Discrete Element Model (DEM). The dynamic source effects explain qualitatively the complex damage distribution caused by this earthquake. The source model for estimating broad-band ground motions (0.1 ~ 20Hz) in near-source area during the 1999 Chi-Chi earthquake is constructed combining the kinematic source process from the waveform inversion with the dynamic rupture process from the forward modeling to fit the synthetics to the observation. The best-fit source model between the synthetic and observed motions consists of a large asperity with an area of 30 × 24km^2 and stress drop of 200 bars at the northern part of the causative fault and smaller two asperities at the southern part near the epicenter, one with an area of 10 × 10km^2 and stress drop of 150 bars and the other with an area of 10 × 14km^2 and stress drop of 150 bars, respectively. We find that the acceleration and velocity waveforms and the acceleration response spectra of the synthetic motions agree well with those of the observed ones. The waveforms at the southern part are composed of rich high-frequency motions with long duration, because the sites are located in the backward direction of those three asperities. The velocity waveforms at the northern sites close to the northern edge of the causative fault make a single large pulse with duration of about 10 sec, being indicative of the forward rupture directivity due to a large asperity in the northern part of the causative fault.

INTRODUCTION

The Chi-Chi (Taiwan) earthquake (Mw = 7.6) of September 20, 1999 had a great impact on the international community of scientists and engineers devoted to seismology and earthquake engineering. The earthquake was one of the most destructive and largest earthquakes in this century. The death toll was more than 2,470 and serious destruction of buildings reached several thousands [1]. The rupture of the causative fault extended about 80km along the Chelungpu fault with significant surface breaks as shown in Fig. 1(a), forming a low-angle reverse fault with a strike or nearly N5°E and a dip between 25° and 36° [2]. The maximum horizontal displacements up to 9.0m and vertical offsets of 1.0m to 4.0m were observed along the surface rupture.

Strong motions during the mainshock were recorded at sites in the near-source area as well as at sites over Taiwan with totally 420 digital accelerographs. It is the first experiences in the world to obtain such great records. The strong motion records showed several significant features. Ground motions in the hanging wall side are larger in general than those in the footwall side. Long period motions dominate at the northern part of the causative fault having large velocity with about 300cm/s in maximum horizontal motion. On the other hand, ground motions at the southern part of the causative fault near the epicenter are predominant in the short period, showing large accelerations with about 1,100 gals in the maximum horizontal motion. Although the strongest velocity motion occurred at the northern part of the fault trace, structural damage seemed to be heavier in the southern part than in the northern part.

Such difference in the damage distribution can be inferred from Fig. 1(b), which shows a comparison of the pseudo-velocity response spectra from records of stations located at the northern (TCU052) and southern (TCU129 and TCU089) parts. The velocity responses at periods longer than 1.0sec are significantly larger in the northern part than those in the southern part. On the contrary, those at periods shorter than 1.0sec are larger in the southern part than in northern parts. The rupture process from the kinematic waveform inversion using the strong ground motion [3] shows the concentration of large asperities in the northern part and small in the southern part (Fig. 2). It seems not clearly to explain the features of ground motion distribution and the damage pattern during he mainshock.

In order to get better understanding of the complex damage distribution caused by this earthquake, we have attempted to simulate the dynamic rupture process and near-source ground motion during the mainshock. Since the faulting process appears to have been nearly pure thrust along the fault segments near the hypocenter, we used a 2D Discrete Element Model (DEM) to perform a dynamic simulation of the rupture process of the causative fault.

We made a simulation of broad-frequency-bank ground motion (0.1 to 20Hz) using a kinematic source model characterized by waveform inversion, taking into account the results from the dynamic rupture process mentioned above. The source process is modeled by the global and local source parameters. The global parameters

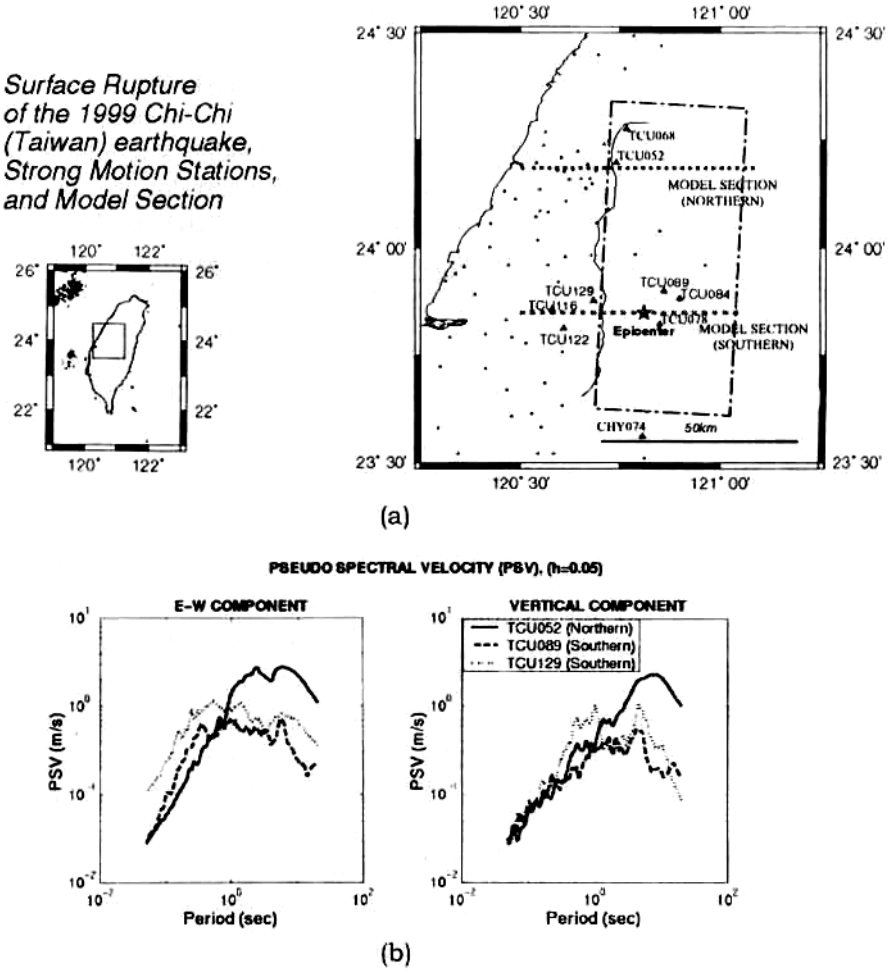

Fig. 1 (a) Location of the surface rupture of the Chelongpu fault, stations records used for comparison, source model and sections of the northern and southern model; (b) Comparison of pseudo spectral velocity for records of stations at the northern and southern parts

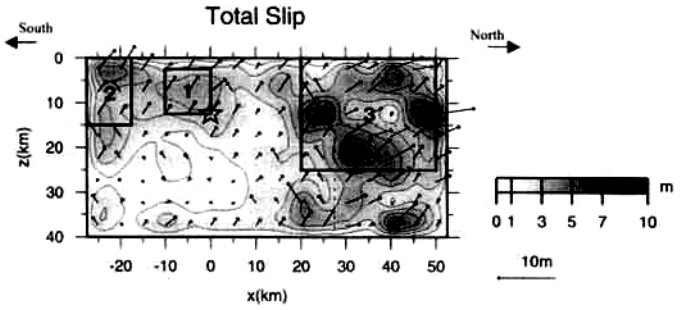

Fig. 2 Fault source model got from the kinematic waveform inversion using the strong ground motion record [3]. Total Moment: 1.60×10^{27} dyne-cm; Rupture area: 3,200km^2 (80km × 40km); Asperity area: 450km^2; Average slip in rupture area: 245cm

such as total rupture area and seismic moment. The local source parameters are slip heterogeneity on fault plane determined from the source inversion. Ground motions are simulated using the hybrid method, deterministic and stochastic approaches in low (< 1Hz) and high (> 1Hz) frequency ranges, respectively, to obtain broad-bank ground motions (Irikura and Kamae, 1999).

We compared the global and local source parameters for the best-fit source model with the scaling relations of rupture areas and asperities so far obtained based on the statistical analysis of the kinematic source inversion for crustal earthquake [4]. For mitigating earthquake damage for future large earthquakes, we need to know how to predict strong ground motion for similar active-fault earthquakes. To do that, we discuss the source model here obtained relating to the source characterization in a recipe for predicting strong ground motion we have proposed [5].

DYNAMIC SOURCE EFFECTS ON STRONG GROUND MOTION

Dynamic Source Model

We make a numerical simulation of the dynamic rupture process and strong ground motion using a 2D Discrete Element Model (DEM). Taking into account the differences in the observed features of the rupture process at the northern and southern parts of the causative fault, each part was modeled independently. The problem is solved in a plane strain condition. The location of the two model sections along the surface rupture is shown in Fig. 1(a). The first model (southern part) is for the epicentral area near TCU084, TCU089, TCU122, and TCU116. The second model (northern part) is near TCU052. The 2D Model is available to perform a dynamic simulation of the rupture process on the fault plane and the near-fault ground motion for the southern part since the faulting process appears to have been nearly pure thrust along the fault segments near the epicentral area. However, the strike-slip component against the dip-slip increases in the northern part [3]. We simulate the second model for the northern part to discuss qualitatively the differences of fault slip and strong motion characteristics between the southern and northern parts.

The parameters used for the dynamic simulation and the geometry of the two fault models are shown in Fig. 3. Both models share the following common assumptions: (1) There is a surface sedimentary layer with a depth of 4km characterized by a set of P wave velocity (4.3km/sec), S wave velocity (2.5km/sec), density 2500kg/m^3. The basement (seismogenic zone) is a homogeneous medium with P wave velocity (6.1km/sec), S wave velocity (3.5km/sec), density 2700km/m^3. (2) The slip-weakening friction model is adopted as the constitutive relation for the fault. (3) The stress drop along the fault plane in the shallow surface layer is negligible. (4)The ultimate stress, i.e., the strength excess on the fault surface in the shallow surface layer increases linearly with depth and, in order to avoid any fault opening, we applied a normal stress along the fault, equivalent to the strength excess. (5) The critical slip (Dc) along the fault is larger near the surface than at greater depths.

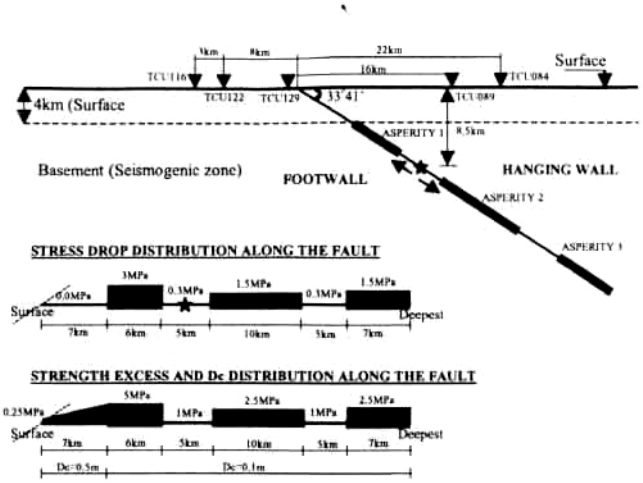

(a) southern model

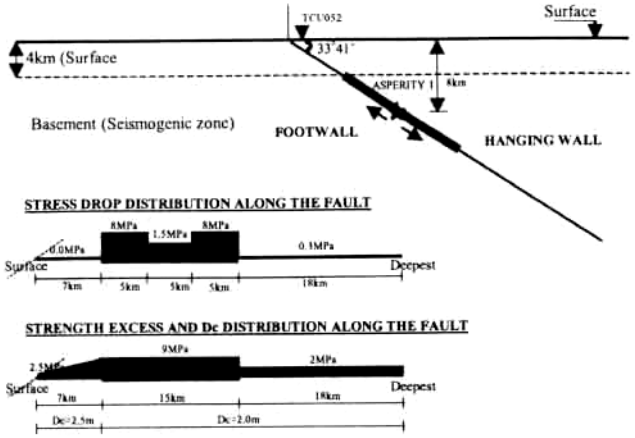

(b) northern model

Fig. 3 Fault models and parameters distribution used for the dynamic simulation

We assume the existence of three asperities with different stress drops for the southern part. An asperity in a shallow part in the basement underlying the sediments has the largest stress drop of 3MPa and other two asperities in deeper parts have smaller stress drop of 1.5MPa. The width of the asperities is relatively small (about 7km) for the southern part compared with that for the northern part. The northern part, on the other hand, is assumed to have just one asperity with larger width (15km) and higher stress-drop (between 1.5MPa and 8MPa).

Simulation Results

The slip and slip velocity distribution along the fault shown in Fig. 4(a) (southern model) and Fig. 4(b) (northern model) suggest that final slip is larger in the northern model than in the southern model. The peak slip velocity at the asperities in the southern model is

reached suddenly as a damped step function similar to the Kostrov's pulse (Kostrov, 1964), that was theoretically obtained in a self-similar shear-crack propagation, however, even the northern model also shows this sudden increasing of the slip velocity in the beginning of the rupture, the peak value is reached smoothly after this step. These results suggest that the rupture process in the southern model is rougher than the northern model, even the slip velocity near the surface is larger in the northern model than in the southern model.

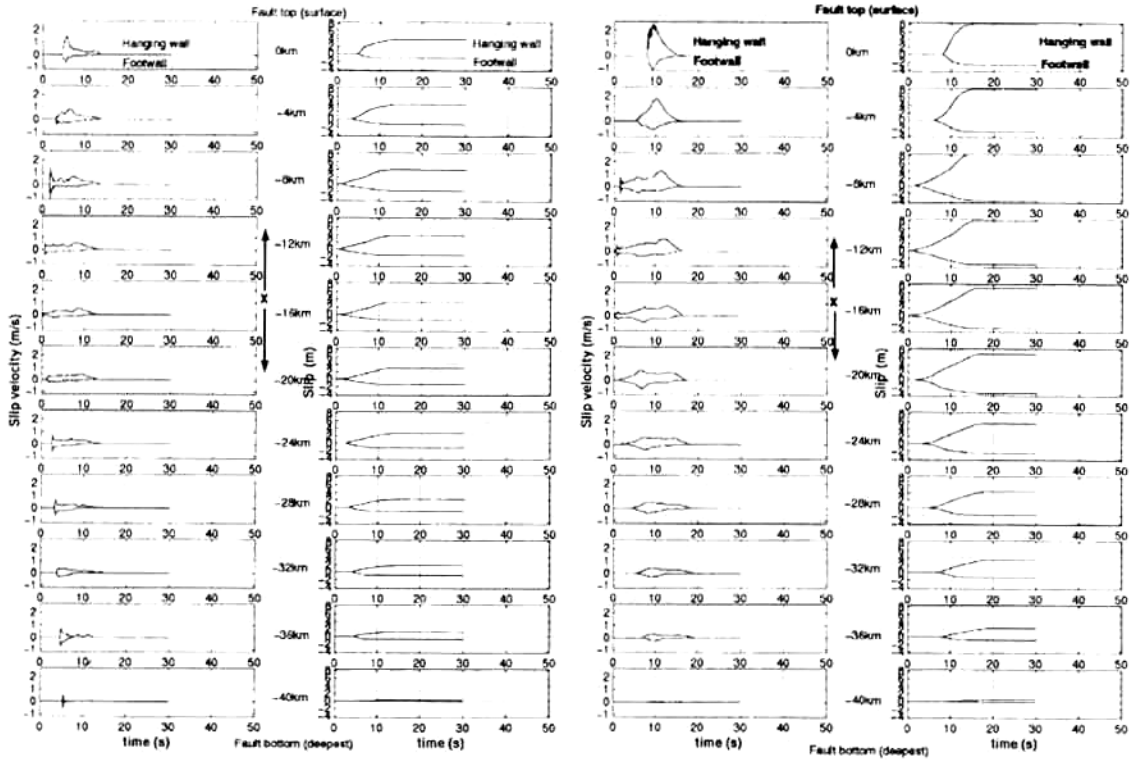

(a) southern model (b) northern model

Fig. 4 Slip and slip velocity along the fault

The ground motions on the surface simulated in a frequency range up to 2.0Hz in the southern model are compared with those in the northern model in Fig. 5. We find that the final displacement and the peak velocity are larger in the northern model than in the southern model in Fig. 5(a) and Fig. 5(b). However, the peak values of the velocity motions filtered in a frequency range of 0.5 to 2.0Hz are larger in the southern model than in the northern model as shown in Fig. 5(c). These results suggest that the northern model generates larger ground motions than the southern model at lower frequencies, while higher frequency motions between 0.5 to 2.0Hz (natural frequency range of standard structures) are larger in the southern model than in the northern model. We can conclude that even if the northern model shows apparently larger ground motion than the southern model, heavier damage in structures could

happen in the southern model because the southern model has more possibilities to excite high frequency motions including the fundamental frequencies (0.5 to 2.0Hz) of standard structures.

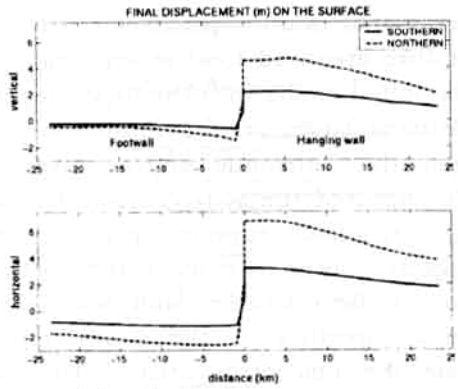

(a) final displacement

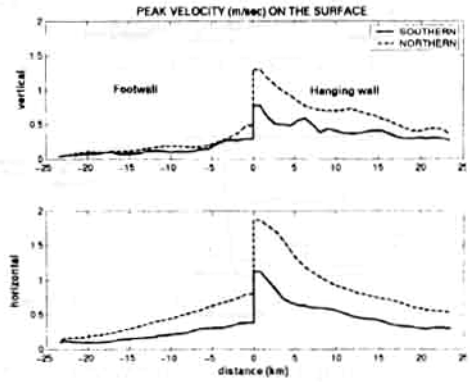

(b) peak velocity

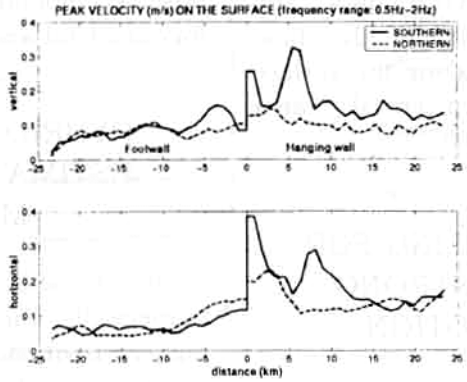

(c) peak velocity in a frequency range of 0.5 ~ 2.0Hz

Fig. 5 Comparison of the final displacement and peak velocity on the surface between the northern model and southern model

In order to validate the dynamic model studied here, we compared our results with the observations. Figure 6 shows that the southern model produces final vertical displacement of about 2.0m and horizontal displacement of about 3.3m in the hanging wall that agree satisfactorily with those obtained by the GPS data and the permanent displacements obtained from the strong motion records. In Figs. 7(a) to 7(e) we also compare the waveform of the displacement and velocity ground motions of east-west and vertical components recorded at five stations near the surface rupture of the epicentral area (stations TCU084, TCU089 on the hanging wall side and TCU129, TCU116 and TCU122 on the footwall side). We find that the main characteristics of the recorded ground motions are adequately reproduced, as observed in the simulated and observed time-histories in the frequency range lower than 1Hz. For the northern model we succeed in simulating the ground motion recorded at TCU052 as shown in Fig. 7(f).

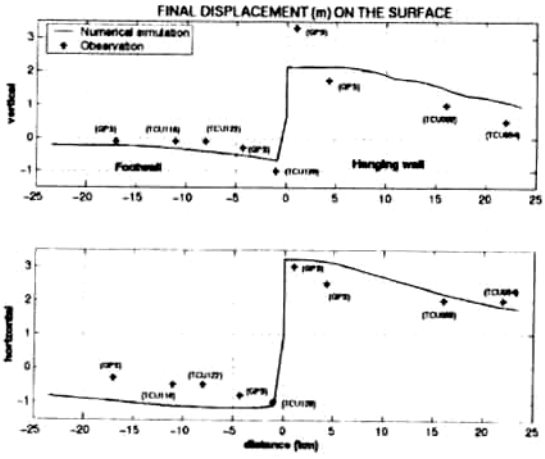

Fig. 6 Comparison between the numerical simulation and the observations (GPS data and stations records) of the final displacements along the surface near the epicentral area (southern model)

SOURCE MODELING FOR SIMULATING STRONG GROUND MOTION

We attempt to make a source model for simulating strong ground motion over a broad-frequency band of engineering interest from 0.1 ~ 20Hz. Many authors have been studying the rupture process of this earthquake from the kinematic inversion of strong ground motion records [3] and also the joint inversion of strong ground motion, teleseismic, and geodetic data [6]. However, these models are not available yet for estimating high-frequency strong ground motions because they are derived from low-frequency data at most 1Hz. We use the hybrid method for estimating broad-band ground motions in deterministic and stochastic approaches in low (< 1Hz) and high (> 1Hz) frequency ranges, respectively. To make a simulation of such broad-bank motions, we need to take into account the local source parameters such as slip heterogeneities, i.e., asperities, as well as the global source parameter such as rupture area and total seismic moment. The initial model with the asperities was assumed based on the rupture process from the kinematic source inversion. We improved the source model learning the dynamic rupture process that suggest a large asperity in the northern part of the causative fault and several small asperities in the southern part near the epicentral area. The best model to fit of synthetic motions to the observed motions is determined using a forward trial-and-error approach.

HYBRID METHOD FOR ESTIMATING GROUND MOTIONS

It is still difficult to compute numerically the Green's functions in higher frequency range (> 1Hz) of engineering interest. We need to have detailed geophysical informations from source to site to compute such high frequency motions. Even if it could be done, another problem is how to compute ground motions in such fine meshed 3D structure. It is required to use so large memory and time-consuming computer. We consider that complete numerical calculation of the Green's function in the broad-frequency band is still economically unrealistic.

For low frequency motion less than 1Hz, we calculate ground motions directly from characterized source model of the mainshock in the flat multi-layered media from source to site by the frequency-wavenumber algorithm (Saikia, 1994) because we do not have

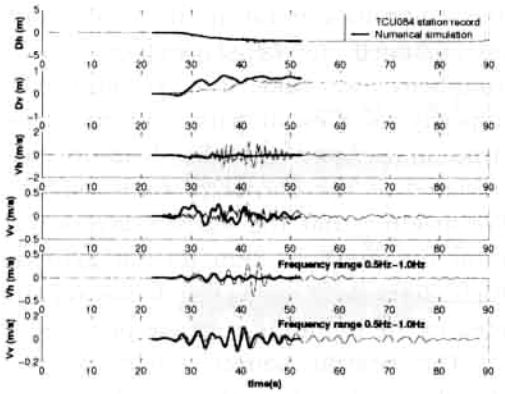

(a) for TCU084 station

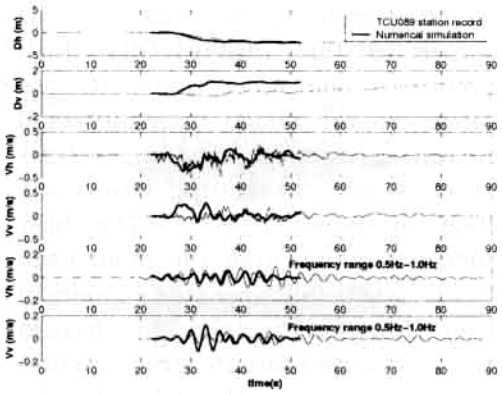

(b) for TCU089 station

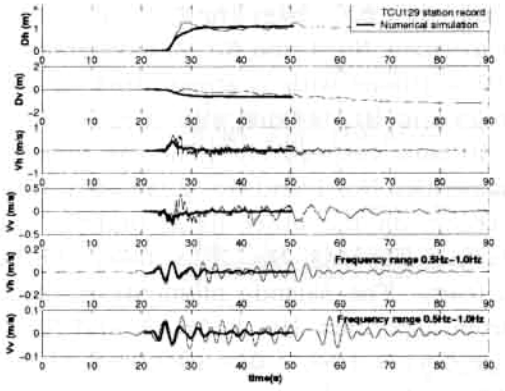

(c) for TCU129 station

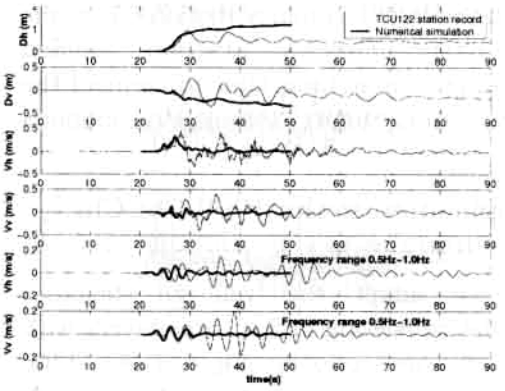

(d) for TCU122 station

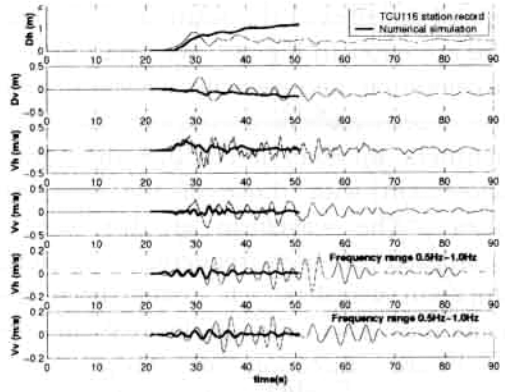

(e) for TCU116 station

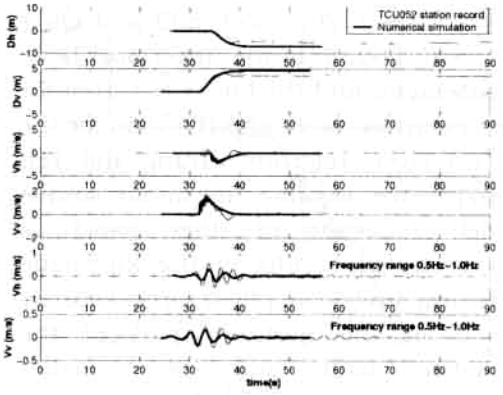

(f) TCU052 station

Fig. 7 Comparison of the numerical simulation with stations records of horizontal (E-W) and vertical component of displacement, velocity and velocity in frequency range of 0.5Hz to 1.0Hz. *Dh* and *Dv* are the horizontal (east-west) and vertical component respectively and *Vh* and *Vv* are the horizontal (east-west) and vertical component of velocity ground motion respectively

information enough to model the 3D structure in this region. For high frequency motion more than 1Hz, we simulate ground motion from the small event with an appropriate size ($2 \times 2km^2$ in this study) using the stochastic method by Boore (1983). The high frequency motions from the mainshock are calculated following the empirical Green's function method by Irikura (1986). Then we compute strong ground motions from large earthquakes for the target source areas summing the low frequency motions numerically simulated and the high frequency motions from the stochastic Green's function method through a matching filter to connect the low and high frequency motions smoothly.

Application to the 1999 Chi-Chi Earthquake

We adopt the velocity structure model consisting of flat three-layers with the S wave velocity Vs = 1.96, 2.56, 3.29km/s, P wave velocity Vp = 3.48, 4.55, 5.85, density ρ = 2.4, 2.5, 2.6g/cm^3, constant attenuation factors of the S and P waves Qs = 200, 250, 500 and Qs = 400, 500, 500, from the uppermost layer to basement, and thickness H = 1km for the uppermost layer and H = 2km for the second layer, referring Chung and Yeh (1997). We assume an initial source model consisting of three asperities based on the results of the kinematic waveform inversion [3], a large asperity No. 3 in the northern part of the causative fault and two smaller asperities No. 1 and No. 2 in southern part near the epicentral area as shown in Fig. 2. We assumed a rake angle of 60° for the subfaults of the asperities No. 1 and No. 2 in the southern part and a rake angle of 45° for those of the asperity No. 3 in the northern part. The size of the subfaults generating the small events is assumed to be $2 \times 2km^2$. For simplicity, we take into account each asperity as a event with uniform stress drop in a finite extent. Rupture was initiated at the corner of each asperity. We assume that the surface layers with total thickness of 3km do not generate high frequency motions following the idea of the dynamic rupture process.

The best-fit source model between the observed and synthetic motions is as follows. The maximum asperity No. 3 has an area of $30 \times 24km^2$ with stress drop of 200 bars and smaller two asperities, No. 1 and No. 2, have areas of $10 \times 10km^2$ with a stress drop of 150 bars and $10 \times 14km^2$ with stress drop of 150 bars, respectively. The rise time for asperities No. 1 and No. 2 is taken to be 0.6sec, on the other hand that for the largest asperity No. 3 is taken to be 2.0sec. The seismic moments released from asperities, No. 1, No. 2, and No. 3 are 0.41×10^{25}, 1.0×10^{25}, and 11.0×10^{25} dyne-cm, respectively. The synthetic motions are compared with the observed ones at TCU078 (see Fig. 1), one of the sites at the southern part near the epicenter in Fig. 8. We find that the acceleration and velocity waveform and the acceleration response spectra of the synthetic motions at TCU078 show good agreement with those of the observed ones. The waveform at this site is composed of high-frequency and long duration wavelets. It comes from the fact that this site is located in the backward direction of those three asperities. We also show the comparison between the observed and synthesized seismograms (velocity waveforms and acceleration response spectra) at TCU068, one of the northern sites close to the northern edge of the Chelungpu fault, in Fig. 9. The velocity

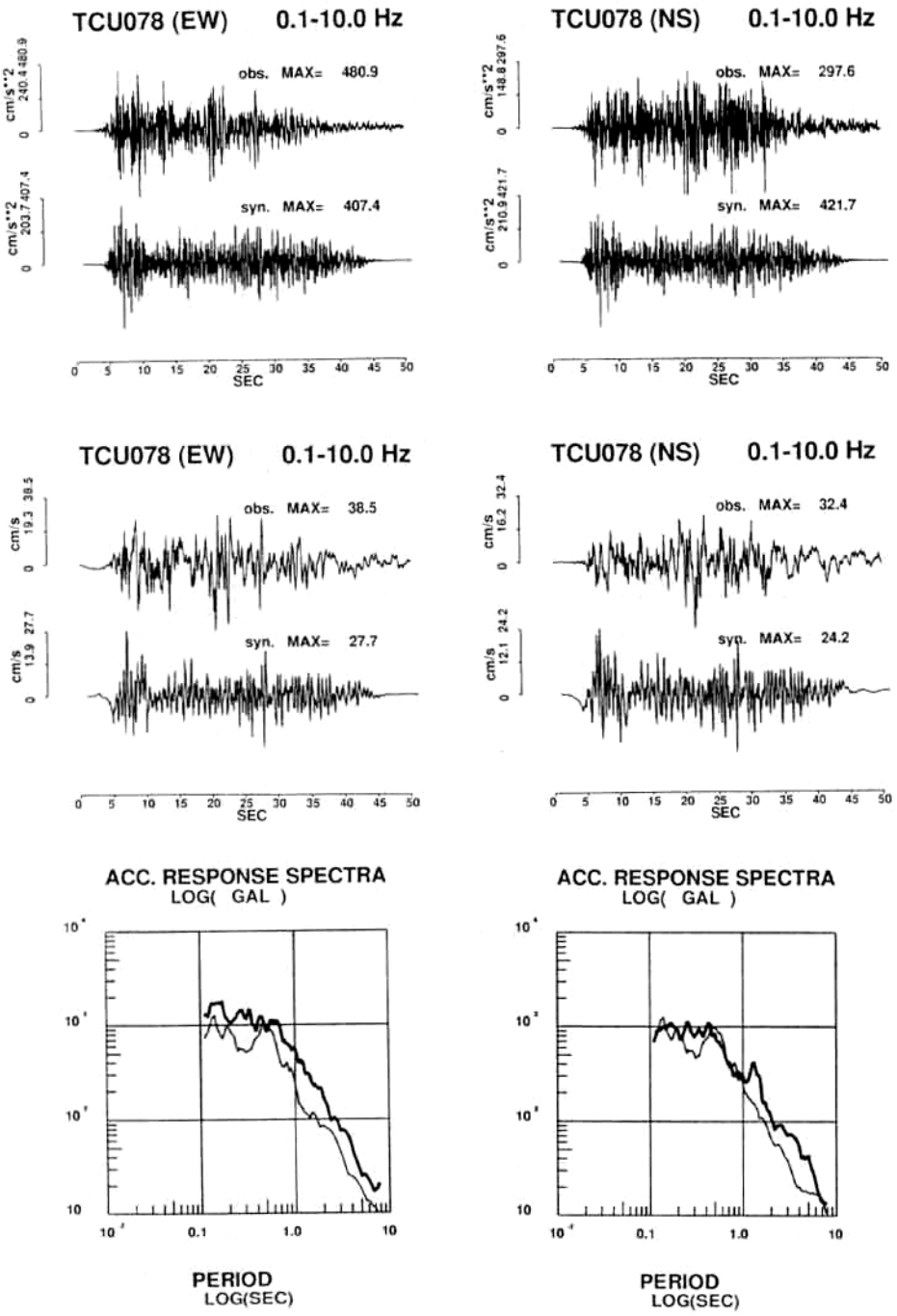

Fig. 8 Comparison between the synthetic acceleration and velocity seismoghrams (EW component close to fault normal, NS component close to fault parallel) and acceleration response spectra using hybrid method and the observed ones at TCU078. This site is located close to the epicenter at the southern part of the causative fault

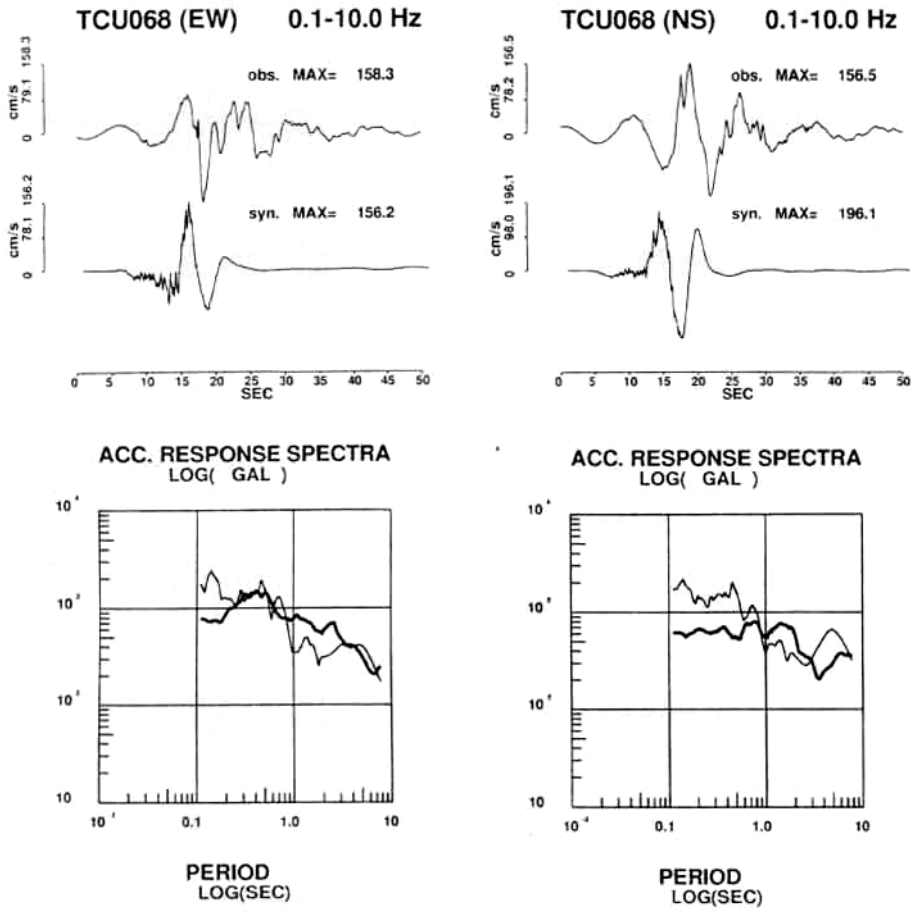

Fig. 9 Comparison between the synthetic velocity seismograms (EW component close to fault normal, NS component close to fault parallel) and acceleration response spectra using hybrid method and the observed ones at TCU068. This site is located at the northern part of the causative fault

motions synthesized here as well as those observed at TCU068 are composed on a single large pulse with duration of about 10sec. This pulse is indicative of the forward rupture directivity due to a large asperity of No. 3. Similar large pulses in the near-source area were observed during the 1992 Landers earthquake in California, USA and the 1995 Hyogo-ken Nanbu earthquake. The predominant periods of the near-source pulses in forward rupture direction depends on the asperity size and slip duration (Irikura, *et al.*, 1996; Somerville, *et al.*, 1996).

The area of the combined asperities is 960km^2, about 30% of the total rupture area. The sum of the seismic moments from those three asperities is about 1.3×10^{25} dyne-cm, about 50% of total seismic moment of the mainshock estimated from the joint inversion of the near-field strong motion data and the teleseismic data [6]. The rate of the area of the combined asperities to the total rupture area is a little high compared

with the average rate from the kinematic source inversion of the crustal earthquakes by Somerville, *et al.* [7]. The rate of the seismic moment of the combined asperity to the total one from the whole rupture area is also a little high compared with the average.

CONCLUSION

We studied some aspects of the dynamic source effects on the strong ground motion of the 1999 Chi-Chi (Taiwan) earthquake using the simplified 2D discrete element method. The ground motions simulated assuming the 2D pure-dip model for the southern part near the epicenter have a satisfactory agreement with the records observed there. The simulation at the TCU052 at the northern part of the causative fault also shows a good agreement with the observation even if the 2D model for simulating ground motion at the northern part is not proper. The results show that the velocity ground motions in the northern part (hanging wall) in the frequency range of 0.5 ~ 2Hz (natural frequency range of standard structures) are small near the surface break, then light structural damage might be predicted near the surface rupture qualitatively. The ground motion in the southern part in the frequency range of 0.5 ~ 2Hz is larger than in the northern part, although the model of the southern part generate smaller ground motions in displacement and velocity than that of the northern part. The dynamic models presented in this paper showed that the effects of the dynamic source mechanism on strong ground motion prediction are the fundamental importance to the assessment of seismic hazard. We find that the acceleration and velocity waveform and the acceleration response spectra of the synthetic motions at both of the southern part near the epicenter agree well with those of the observed ones. The waveforms at the southern part are composed of high-frequency motions with long duration, because the sites are located in the backward direction of those three asperities. The velocity motions at the northern sites close to the northern edge of the causative fault are composed of a single large pulse with duration of about 10sec, being indicative of the forward rupture directivity due to a large asperity in the northern part of the fault.

The rate of the area of the combined asperities to the total rupture area is a little high compared with the average rate from the kinematic source inversion of the crustal earthquakes by Somerville, *et al.* [4]. The rate of the seismic moment of the combined asperity to the total one from the whole rupture area is also a little high compared with the average. Such informations are very important to characterize the source model for predicting strong ground motion for similar active-fault earthquakes in future.

ACKNOWLEDGEMENTS

We thank the Seismology Center, Central Weather Bureau (CWB), Taipei, Taiwan for providing the Digital waveform files corresponding to the accelerograms of the stations used.

REFERENCES

1. Yeh, Y.H. (2000). "The Chi-Chi earthquake in Taiwan," *2000 Western Pacific Geophysics Meeting, Published*

as a Supplement to EOS, Transaction, AGU, 81, WP104, S21A-01 (abstract), Tokyo, Japan, June 27~30.

2. Shin, T.C., Kuo, K.W., Lee, W.H.K., Teng, T.L. and Tsai, Y.B. (2000). "A preliminary report on the 1999 Chi-Chi (Taiwan) earthquake," *Seismological Research Letters*, Vol. 71, pp. 24–30.
3. Iwata, T., Sekiguchi, H. and Irikura, K. (2000). "Rupture process of the 1999 Chi-Chi, Taiwan earthquake and its near-fault strong ground motion," *International Workshop on Annual Commemoration of Chi-Chi Earthquake*, Taipei, Taiwan, R.O.C., September 18~20.
4. Somerville, P., Irikura, K., Graves, R., Sawada, S., Wald, D., Abrahamson, N., Iwasaki, Y., Kagawa, T., Smith, N. and Kowada, A. (1999). "Characterizing crustal earthquake slip models for the prediction of strong ground motion," *Seismological Research Letters*, Vol. 70, No. 1, pp. 59–80.
5. Irikura, K. (2000). "Prediction of strong motions from future earthquakes caused by active faults — case of the Osaka basin," *Proceedings of 12th World Conference Earthquake Engineering*, CD-ROM.
6. Yagi, Y. and Kikuchi, M. (2000). "Source rupture process of the Chi-Chi, Taiwan, earthquake of 1999, obtained by seismic wave and GPS data," *2000 Western Pacific Geophysics Meeting, Published as a Supplement to EOS, Transaction, AGU*, 81, WP104, S21A-05 (abstract), Tokyo, Japan, June 27~30.
7. Somerville, P., Irikura, K., Graves, R., Sawada, S., Wald, D., Abrahamson, N., Iwasaki, Y., Kagawa, T., Smith, N. and Kowada, A. (1999). "Characterizing crustal earthquake slip models for the prediction of strong ground motion," *Seismoloical Research Letters*, Vol. 71, No. 1, pp. 59–80.
8. Kamae, K., Irikura, K. and Pitarka, A. (1998). "A technique for simulating strong ground motion using hybrid Green's function," Bull. Seism. Soc. Am., Vol. 88, pp. 357–367.
9. Saikia, C.K. (1993). "Modified frequency-wavenumber algorithm for regional seismograms using Filon's quadrature: modeling Lg waves in North America," *Geophysical J. Intern.*, Vol. 118, pp. 142–158.
10. Yagi, Y. and Kikuchi, M. (2000). "Source rupture process of the Chi-Chi, Taiwan, earthquake of 1999, obtained by seismic wave and GPS data," *2000 Wetern Pacific Geophysics Meeting, Supplement to EOS, Transaction, AGU*, 81, WP104, S21A-05 (abstract), Tokyo, Japan, June 27~30.
11. Yehc, Y.H. (2000). "The Chi-Chi earthquake in Taiwan," *2000 Western Pacific Geophysics Meeting, Supplement to EOS, Transaction, AGU*, 81, WP104, S21A-01 (abstract), Tokyo, Japan, June 27~30.
12. Shin, T.C., Kuo, K.W., Lee, W.H.K., Teng, T.L. and Tsai, Y.B. (2000). "A preliminary report on the 1999 Chi-Chi (Taiwan) earthquake," *Seismological Research Letters*, Vol. 71, pp. 24–30.